THE EUROPEAN
PHYSICAL JOURNAL D

Regular Article

An (e, 2e + ion) study of electron-impact ionization and fragmentation of tetrafluoromethane at low energies

Khokon Hossen[1,2], Xueguang Ren[1], Enliang Wang[1], S.V.K. Kumar[3], and Alexander Dorn[1,a]

[1] Max Planck Institute for Nuclear Physics, 69117 Heidelberg, Germany
[2] University of Santiago de Compostela (USC), 15782 Santiago de Compostela, Spain
[3] Tata Institute of Fundamental Research, Homi Bhabha Road, Colaba, Mumbai 400 005, India

Abstract. We study ionization and fragmentation of tetrafluoromethane (CF_4) molecule induced by electron impact at low energies ($E_0 = 38$ and $67\,\mathrm{eV}$). We use a reaction microscope combined with a pulsed photoemission electron beam for our experimental investigation. The momentum vectors of the two outgoing electrons (energies E_1, E_2) and one fragment ion are detected in triple coincidence (e, 2e + ion). After dissociation, the fragment products observed are CF_3^+, CF_2^+, CF^+, F^+ and C^+. For CF_3^+ and CF_2^+ channels, we measure the ionized orbitals binding energies, the kinetic energy (KE) of the charged fragments and the two-dimensional (2D) correlation map between binding energy (BE) and KE of the fragments. From the BE and KE spectra, we conclude which molecular orbitals contribute to particular fragmentation channels of CF_4. We also measure the total ionization cross section for the formation of CF_3^+ and CF_2^+ ions as function of projectile energy. We compare our results with earlier experiments and calculations for electron-impact and photoionization. The major contribution to CF_3^+ formation originates from ionization of the $4t_2$ orbital while CF_2^+ is mainly formed after $3t_2$ orbital ionization. We also observe a weak contribution of the $(4a_1)^{-1}$ state for the channel CF_3^+.

1 Introduction

Electron-impact ionization of atoms and molecules plays an important role in a large range of scientific and practical areas like radiation chemistry, reactive plasmas, planetary atmospheres, environment and medical radiotherapy [1]. In case of molecules, ionization may populate dissociative states and finally result in positively charged and neutral fragments.

Tetrafluoromethane (CF_4) is one of the major fluorine containing molecules which is very important in semiconductor industry and used in etching processes [2]. It is an interesting molecule because of having high chemical stability, a high degree of symmetry and unusual dissociative behavior of its ionic fragments [3–5]. The absorption ability of infrared radiation of this molecule is large and consequently, it is a potent greenhouse gas and in the earth atmosphere it contributes to the global warming.

Various experiments and calculations have been done on CF_4 molecules with different experimental and theoretical methods to study the electronic structure, the various ionization channels, partial and total ionization cross sections, generalized oscillator strengths, and orbital momentum densities. Studies of photon induced reactions include fluorescence measurements [6], photoabsorption [7], photoelectron spectrometry [8–14], threshold photoelectron spectroscopy (TPES) [15–18], photoion detection [19,20] and various coincidence methods like photoelectron–photoion coincidences (PEPICO) [21–24], threshold photoelectron–photoion coincidences (TPEPICO) [4,25,26] and threshold photoelectron–fluorescence coincidences (TPEFCO) [5]. Photo double ionization was studied using photoion–photoion coincidences (PIPICO) [27–29], photoelectron–photoelectron coincidences (PEPECO) [30] and threshold photoelectron–photoion–photoion coincidences after core ionization (TPEPIPICO) [31]. There are also studies reported on negative ion fragment formation by photons [32].

Electron impact studies include measurements on electron energy loss [33–41], excitation [42], ionization observing total [43,44], total dissociation [45] and partial ionization cross sections using fragment ion mass analysis [42,46–52]. Furthermore, binary (e, 2e) studies [53,54] and electron impact fragment ion–photon coincidences (FIPCO) [55] were performed. However, to the best of our knowledge there are no experiments on electron impact induced fragmentation of CF_4 where the binding energies and, therefore, the ionized orbitals leading to particular fragment ions are resolved and identified. This is possible only in (e, 2e + ion) triple coincidence measurements where the energies of both outgoing electrons as well as the energy and the charge to mass ratio of the fragment ion are measured.

[a] e-mail: alexander.dorn@mpi-hd.mpg.de

Here, we report measurements on the ionization and fragmentation of CF_4 at low electron impact energies ($E_0 = 38$ and $67\,eV$) using the triple coincidence method (e, $2e + $ ion) in which two outgoing electrons (energies E_1 and E_2) and one fragment ion are detected. The two projectile energies were chosen to see cross section dependences on impact energy and, furthermore, to obtain information on a suspected resonance in the CF_2^+ ion yield near $38\,eV$ impact energy.

For the CF_4 molecule, this experimental method is used for the first time. For the CF_3^+ and CF_2^+ fragment ions, their momentum vectors, the ionized orbital binding energies (BE) and kinetic energy release (KER) values are measured. Furthermore, the correlation map between BE and KER for each product are obtained. We can define the binding energy E_b as

$$E_b = E_0 - E_1 - E_2. \qquad (1)$$

Here, E_0 is the initial projectile energy, E_1 and E_2 denote the energies of the two outgoing electrons (scattered electron and ejected electron). The BE is the vertical transition energy required to ionize a particular electronic orbital [56–58].

The summation of the kinetic energies of the ion and the neutral fragments formed in the dissociation process is the KER. The KER reveals the nature of the ground state wave function of the molecule and also the shape of the potential energy surfaces in which the ion has been formed. The kinetic energy released is given by

$$\mathrm{KER} = \frac{\vec{P}_{\mathrm{ion}}^2}{2m_{\mathrm{ion}}} + \sum \frac{\vec{P}_{\mathrm{neutral\,fragmnet}}^2}{2m_{\mathrm{neutral\,fragment}}}. \qquad (2)$$

In case of a two-body decay, the momentum of the ion and that of the neutral fragment is equal but opposite. In this experiment, the ionic fragments of CF_3^+, CF_2^+, CF^+, F^+ and C^+ from CF_4 are clearly resolved. We compare our results with electron impact ionization [33,36,47,48,53], and photoionization studies [8,11–13,15,21,22,59].

2 Experimental method

To perform these experiments, we used an advanced reaction microscope which is built especially for electron-impact ionization studies [56,60]. The basic principles of a general reaction microscope have been described by Ullrich et al. [60]. Details of the experimental method are described in one of our earlier studies [56]. Here, we provide a short description on the experimental setup used for the present set of measurements. A well-focused ($\approx 1\,mm$ diameter) and pulsed electron beam of a particular energy crosses a supersonic gas jet. The target gas expands through a nozzle of $30\,\mu m$ diameter, passes two skimmers and finally enters the main scattering chamber. We used a photoemission electron gun in which a tantalum photocathode is illuminated by a pulsed ultraviolet laser with wavelength $266\,nm$ ($\approx 4.66\,eV$) and pulse duration of less than $0.5\,ns$. The electrons are accelerated to form a pulsed electron beam of desired energy which intersects

the molecular beam at $90°$. For ionization the charged particles (two electrons and one ion) are accelerated and guided by homogeneous electric and magnetic fields and finally detected by the electron and ion detectors which are placed opposite to each other.

For each triple-coincidence the particles' times of flight (TOF) and positions on the detectors are measured. In the offline analysis we can obtain the momentum vectors for all particles. The solid angle for the electron detection is almost 4π. In the case of a dissociation process, we can measure the orbital binding energy, the kinetic energy (KE) of the fragment ion and the two-dimensional (2D) correlation map between BE and KE of the fragments.

For the measurement of the total partial ionization cross section as function of projectile energy for the ions CF_3^+ and CF_2^+, we have used the experimental setup described in an earlier study [61].

For calibration of the electron spectrometer, ionization of the argon atoms in the $3p$ orbital with well-known binding energy was used. The full width at half maximum (FWHM) for the $Ar(3p)$ BE is about $2.65\,eV$ which corresponds to BE resolution (ΔE_b) of this experiment at $E_0 = 67\,eV$ [see Fig. 2b inset]. The accuracy of the measured ion kinetic energies ΔE_{KE} is determined by the momentum resolution Δp_{ion} of the ion spectrometer. In the present measurement the ion momentum $p_{\mathrm{ion}}^{\perp}$ transversal to the ion extraction field is determined from ion detection position on the detector and the ion time of flight t_{TOF} according to

$$p_{\mathrm{ion}}^{\perp} = m_{\mathrm{ion}} \cdot r / t_{\mathrm{TOF}}. \qquad (3)$$

Here m_{ion} is the ion mass and r is the ion detection position with respect to the center of the detector where ions with zero initial transversal momentum are detected. The momentum resolution is limited by the size of the ion source volume of about $1\,mm$ which directly translates into the accuracy for the measurement of r and by error propagation to ΔE_{KE}. As result the accuracy of the KER values for CF_3^+ is $\pm 0.08\,eV$. For CF_2^+ the accuracy of the KER is $\pm 0.025\,eV$ while for the CF_2^+ kinetic energy it is $\pm 0.011\,eV$.

3 Results and discussions

The CF_4 molecule has tetrahedral geometry. The ground state electronic configuration of the CF_4 molecule (in t_d symmetry) [10,36,62] is given by

see equation next page

The two lowest unoccupied orbitals (LUMOs) in the ground state of this molecule are $5a_1$ and $5t_2$ [8]. The five outer-valence orbitals are $1t_1$, $4t_2$, $1e$, $3t_2$, and $4a_1$ and their vertical ionization energies are known from high-resolution HeI and HeII Photoelectron Spectra (PES) to be $16.20\,eV$, $17.40\,eV$, $18.50\,eV$, $22.12\,eV$ and $25.12\,eV$ respectively [62]. The vertical ionization energies of the inner-valence orbitals ($2t_2$, $3a_1$) are $40.3\,eV$ and $43.8\,eV$ respectively [59,63]. The three highest occupied molecular

$$\underbrace{(1a_1)^2(1t_2)^6}_{F1s}\underbrace{(2a_1)^2}_{C1s}\underbrace{(3a_1)^2(2t_2)^6}_{\text{inner-valence}}\underbrace{(4a_1)^2(3t_2)^6(1e)^4(4t_2)^6(1t_1)^6}_{\text{outer-valence}}\ {}^1A_1$$
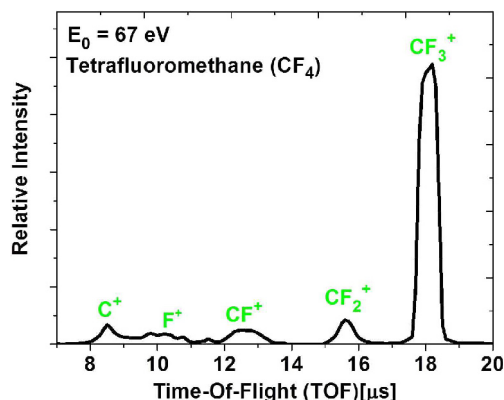
Fig. 1. The experimental time of flight (TOF) spectrum for electron-impact ionization and fragmentation of CF_4 at 67 eV impact energy.

orbitals (HOMOs) are the lone-pair orbitals of the fluorine atoms and lie within an energy range of 2.3 eV. Ionizing one electron from the outer-valence orbitals with increasing binding energy will lead to CF_4^+ in the ionic states $\tilde{X}\ ^2T_1$, $\tilde{A}\ ^2T_2$, $\tilde{B}\ ^2E$, $\tilde{C}\ ^2T_2$ and $\tilde{D}\ ^2A_1$.

3.1 Fragment ion time of flight (TOF) spectrum of CF_4

The time of flight (TOF) spectrum of the ionic fragments observed at the 67 eV electron impact ionization of CF_4 is presented in Figure 1. Ionic fragments, CF_3^+, CF_2^+, CF^+, F^+ and C^+ can be clearly identified. The parent ion CF_4^+ is not observed due to its instability [37,39,48]. According to Stephan et al. [46], Brehm et al. [22] and Fiegele et al. [50], the life time of CF_4^+ ion is below 10 μs. On the other hand, some studies found indications of the existence of the CF_4^+ ion with very small relative intensity [64–67]. In our experiment with a transit time of $\sim$20 μs from the interaction zone to the detector the CF_4^+ ion signal was below the detection limit.

3.2 CF_3^+

For electron impact ionization of the CF_4 molecule the CF_3^+ ion is the main product. It is formed by the loss of one neutral fluorine atom from CF_4 molecule ($CF_4^+ \rightarrow CF_3^+ + F$). The experimental two-dimensional (2D) maps showing the correlation between BE and KER for the CF_3^+ channel are displayed in Figures 2a and 3a for impact energies of $E_0 = 67$ eV and 38 eV, respectively. The pure BE spectra are presented in Figures 2b and 3b for $E_0 = 67$ eV and 38 eV respectively. The calibration of the BE is done by measuring ionization of the Ar(3p) orbital (BE = 15.75 eV). In the inset of the Figure 2b, the BE

histogram of argon is shown for $E_0 = 67$ eV under the same experimental conditions as used for CF_4.

The BE distribution shows a main peak at $\sim$17 eV and a shoulder and a tail at higher energy. The contributions of the individual orbitals are analyzed by a Gaussian multi-peak fitting method. The widths of the Gaussian functions correspond to the experimental resolution and the positions are taken as the literature values of the orbitals' vertical binding energies.

Several ionization channels contribute to form CF_3^+. The dominant peak at 17.4 eV is due to the ionization of the three orbitals $1t_1$, $4t_2$ and $1e$. These three orbitals are energetically not resolved.

The peak observed at 22.12 eV is due to the ionization of the orbital $3t_2$ and partly due to autoionization states [12,15,62]. Interestingly the peak intensity relative to the main peak at 17.4 eV changes with the projectile energy. For $E_0 = 67$ eV the relative intensity is 25% [see Fig. 2b] while for $E_0 = 38$ eV the intensity increases to 36% [see Fig. 3b]. Finally, a third weak contribution at 25.1 eV is due to the ionization of the orbital $4a_1$.

The total KER spectrum and the individual contributions of the different orbitals are shown in Figures 2c and 3c for $E_0 = 67$ eV and 38 eV, respectively. The KER is rather large peaking at around 1.0 eV. At $E_0 = 67$ eV, the mean KER values (uncertainty ± 0.07 eV) for the individual orbitals of $1t_1$, $4t_2$, $1e$, $3t_2$ and $4a_1$, are 1.05 eV, 1.13 eV, 1.17 eV, 1.16 eV and 1.18 eV respectively (uncertainties of all values ± 0.07 eV) while at $E_0 = 38$ eV we find very similar mean KER values of 1.05 eV ($\tilde{X}$), 1.12 eV ($\tilde{A}$), 1.13 eV ($\tilde{B}$), 1.13 eV ($\tilde{C}$) and 1.13 eV ($\tilde{D}$). These KER values are obtained by analyzing the KER spectra for binding energy intervals as given in the caption of Figure 2c. Clearly the present binding energy resolution is not sufficient to completely disentangle the KER spectra of the three lowest states. However, still we can recognize the smaller mean KER of the $1t_1$ orbital in particular with a peak position of the KER distribution at 0.92 eV. The KER curves for the other orbitals are close to each other. Our results are in reasonable agreement with earlier TPEPICO values from Creasey et al. [4] for the two lower states but not for the higher states, where these authors obtained higher mean energies (1.27 ± 0.14 eV ($\tilde{B}$), 1.34 ± 0.10 eV ($\tilde{C}$) and 1.54 ± 0.13 eV ($\tilde{D}$)). One uncertainty there could be the reconstruction of the KER purely from ion time-of-flight and not from the full ion momentum vector as in the present case. A more recent high resolution TPEPICO experiment [25] observed the three lowest states with mean KER values of 0.90 eV, 1.20 eV and 1.09 eV. From the high KER values observed, these studies concluded that both the $\tilde{X}$ and $\tilde{A}$ states dissociate immediately and non-statistically on their individual repulsive potential energy curves leading to slightly different KER, as it is also observed in the present data.
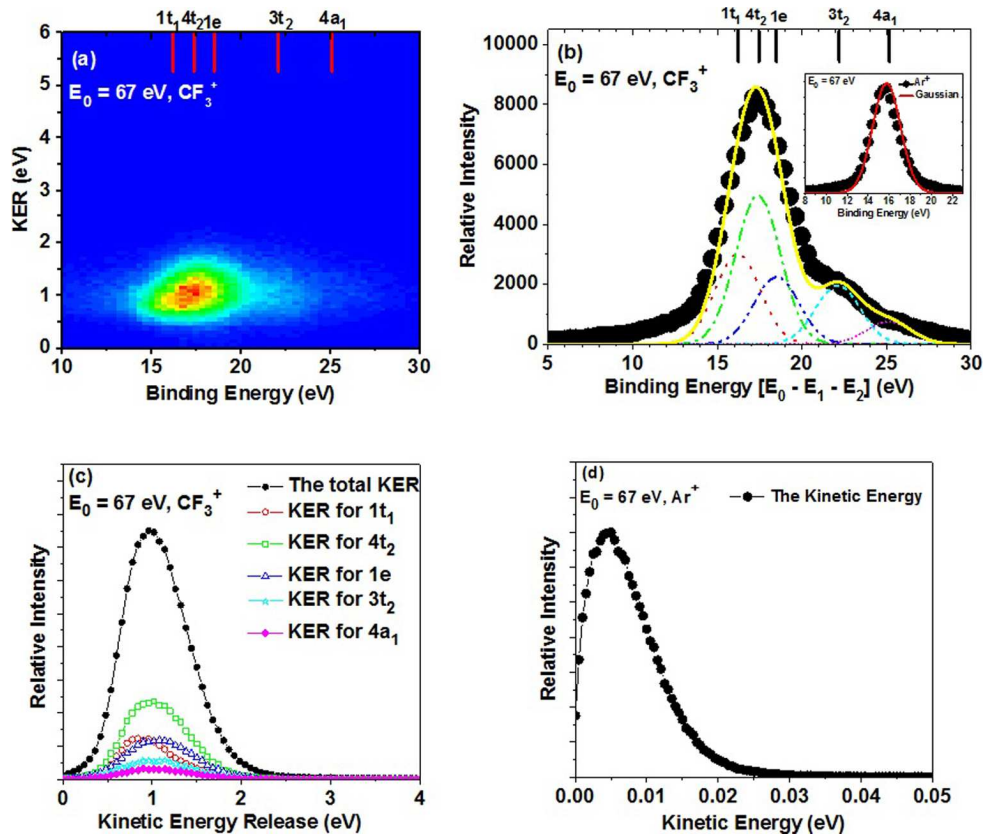
Fig. 2. (a) Two dimensional (2D) correlation map between KER and BE for the CF_3^+ ion at 67 eV impact energy. (b) The binding energy spectrum. The solid circles are the experimental data. The dotted (red), dash-dotted (green), dash-dot-dotted (blue), dashed (cyan) and short-dotted (magenta) lines show the contributions of the orbitals $1t_1$, $4t_2$, $1e$, $3t_2$ and $4a_1$ respectively. The solid line (yellow) shows the sum of the Gaussians. The vertical lines on the top of the figure indicate the energies of the different molecular orbitals that contribute to form CF_3^+ ions. The binding energy diagram for the Ar(3p) orbital is shown in the inset. (c) The total CF_3^+ KER distribution and KER for $1t_1$ (BE: 13–16 eV), $4t_2$ (BE: 16–18.5 eV), $1e$ (BE: 18.5–20.5 eV), $3t_2$ (BE: 21–23 eV), and $4a_1 1$ (BE: 24.5–27 eV) orbitals. (d) The kinetic energy (KE) distribution of Ar^+.

On the other hand, the ionic $\tilde{B}$ state is initially bound. From the observed dissociation with similar KER as observed for the $\tilde{A}$ state it was inferred that there is a transition to this state via fast internal conversion (IC) or radiative decay. Our present data confirm that also the higher lying $\tilde{C}$ and $\tilde{D}$ states which KER values very close to the ones of the $\tilde{A}$ and $\tilde{B}$ states undergo transitions to the ionic $\tilde{A}$ state before they dissociate.

Overall, the ionization of the orbitals $(1t_1)^{-1}$, $(4t_2)^{-1}$, $(1e)^{-1}$ and $(3t_2)^{-1}$ provide the main channels to form the CF_3^+ ion. In addition, a weak contribution of the $(4a_1)^{-1}$ state is observed. Comparing the earlier studies for the formation of the CF_3^+ ion, this is in agreement with TPEPICO studies [4,20,26] while the PEPICO [24] and TPEFCO [?] studies did not identify the weak contribution of the $(4a_1)^{-1}$ orbital. Existing electron impact ionization studies were restricted to the detection of at most two of the three charged fragments. The electron impact dissociative ionization study [48] observed appearance energies and, therefore, discussed only the contribution of the $(1t_1)^{-1}$ state. The dipole (e, e) spectroscopy study [39] proposed that $(1t_1)^{-1}$, $(4t_2)^{-1}$, $(1e)^{-1}$ and $(3t_2)^{-1}$ states contribute to form CF_3^+.

3.3 CF_2^+

The second main product observed is the CF_2^+ ion. This ion can be formed by a two body $(CF_4^+ \rightarrow CF_2^+ + F_2)$ or a three body $(CF_4^+ \rightarrow CF_2^+ + 2F)$ dissociation process. The observed two dimensional (2D) correlational maps between BE and KER are shown in Figures 4a and 5a for $E_0 = 67$ eV and 38 eV, respectively. Here we can identify clearly the reaction channels leading to the CF_2^+ ion. The dominant $3t_2$ orbital ionization gives rise to small KER values while the weaker $4a_1$ contribution shows its main intensity at KER between 1 eV and 2 eV. The binding energy spectrum which is integrated over the KER is presented in Figures 4b and 5b for $E_0 = 67$ eV and 38 eV respectively. This spectrum is analyzed by a Gaussian multi-peak fitting method. For both projectile energies we observed a dominant peak at 22.5 eV BE, which is due to the ionization of the $3t_2$ state. The second peak at 25.5 eV is due to the ionization of the orbital $4a_1$. Interestingly the lower projectile energy shows a reduced relative intensity for $4a_1$ ionization which can be due to approaching the threshold region since here the projectile excess energy is only 12.5 eV.
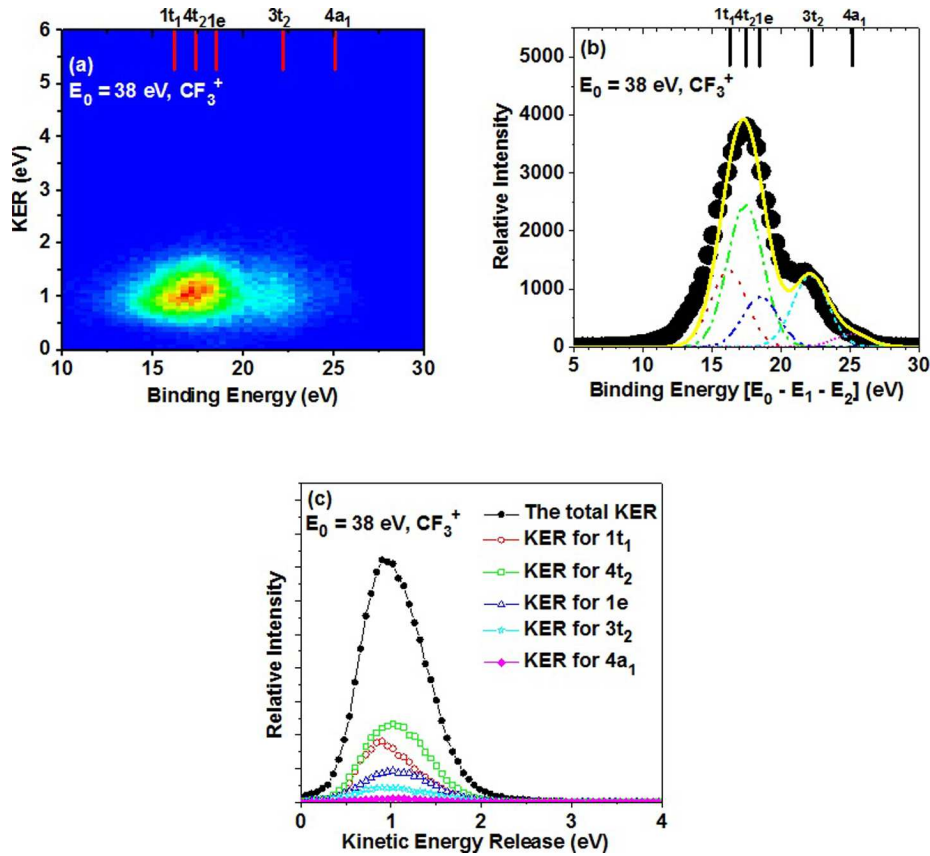
Fig. 3. As for Figure 2a–c but for electron impact energy of 38 eV.

A small contribution with a binding energy lower than 20 eV is also seen [see Figs. 4b and 5b]. Since the lowest dissociation energy into $CF_2^+ + F_2$ is 19.2 eV [4] either high vibrational levels of the $CF_4^+(1e^{-1})$ ion must be excited or autoionization states $3t_2^{-1}$ nl are populated with energies converging to the $CF_4^+(3t_2^{-1})$ state. Autoionizing states in this energy region have been observed before in a photoionization study [12]. For the moment, we label this contribution to the 1e orbital.

The KER is extracted assuming a two body dissociation process $(CF_4^+ \rightarrow CF_2^+ + F_2)$. The KER spectra for 1e, $3t_2$ and $4a_1$ orbitals are shown in Figures 4 and 5c for $E_0 = 67$ eV and 38 eV, respectively. For the orbitals 1e and $3t_2$, we observed average KER of about 0.3 eV ranging up to 1.5 eV and 2 eV respectively. For the higher lying orbital $4a_1$, we observe a different behavior with a strong contribution at around KER = 1.5 eV compared to the 1e and $3t_2$ orbitals. This result agrees with the TPEPICO study [4] which found mean KER values of 0.57 eV and 1.50 eV for the $3t_2$ and $4a_1$ orbitals, respectively.

In Figures 4d and 5d the measured fragment ion CF_2^+ kinetic energy (KE) is presented for $E_0 = 67$ eV and 38 eV, respectively. These spectra are correct irrespective of two- or three-body decay.

Our results are consistent with the TPEPICO studies [4,26]. Masuoka and Kobayashi [20] also observed similar results but did not observe the small contribution of the 1e orbital. The electron impact dissociative ionization study

[48], found appearance energy below 20 eV and concluded the contribution of the $(1e)^{-1}$ state. The dipole (e, e) spectroscopy studies [39] proposed that only ionization of the $3t_2$ state contributes to form the CF_2^+ ion. The PEPICO experiment [24] also did not discuss the contribution of the $(1e)^{-1}$ and $(4a_1)^{-1}$ states.

3.4 Dissociative ionization cross sections

In addition to the above fixed projectile energy studies we also measured dissociative ionization cross sections for formation of the CF_3^+ and CF_2^+ ions as function of impact energy from $E_0 = 15$ eV to 45 eV. The experimental setup used for this measurement is described elsewhere [61]. The relative scale of the cross sections for both ions is fixed. On the other hand our data are not absolutely normalized but scaled for the best fit to published absolute cross sections for electron impact which are shown in Figures 6 and 7 [46,47]. Our ionization cross section for formation of CF_3^+ [Fig. 6] shows a broad resonance structure at around 35.0 eV while this structure is only weakly indicated in the earlier electron impact experiments shown. In this diagram we also made a comparison with a photoionization study which also shows a maximum in the cross section [27].

The partial ionization cross section for CF_2^+ as a function of projectile is shown in Figure 7. We observed a peak structure at around 35.0 eV which is more pronounced and
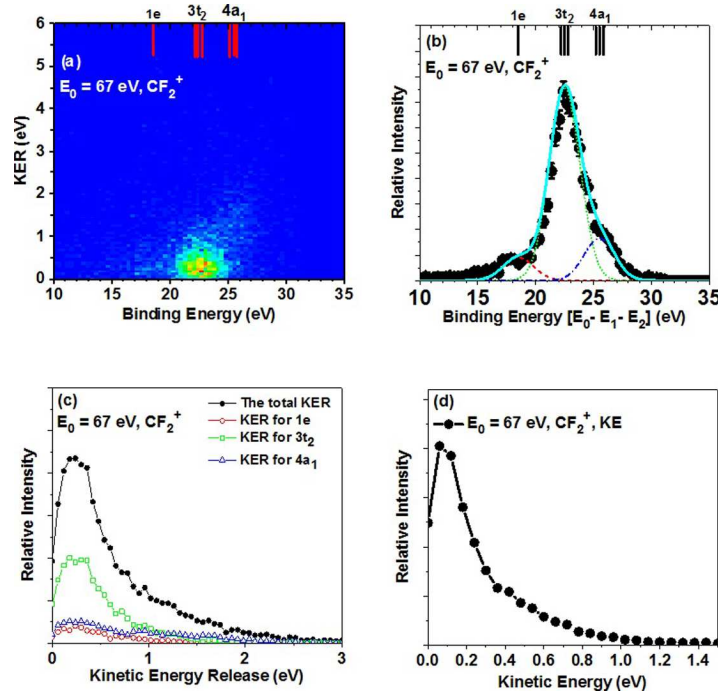
Fig. 4. (a) Two dimensional (2D) correlation map between KER and BE for the CF_2^+ ion at an electron impact energy of 67 eV. (b) The binding energy spectrum. The solid circles with error bars are the experimental data. The dashed (red), dotted (green), and dash-dotted (blue) lines show the contributions of the orbitals 1e, $3t_2$ and $4a_1$ respectively. The solid line (cyan) shows the sum of the Gaussians. The vertical lines on the top of the figure indicate the energies of different molecular orbitals which contribute to the CF_2^+ ion yield. (c) The total KER distribution and KER for 1e (BE: 16–20 eV), $3t_2$ (BE: 20–24 eV) and $4a_1$ (BE: 25–28 eV) orbitals and (d) KE distribution.

broader than the resonance for the CF_3^+ channel. Also here we made a comparison with earlier studies for photoionization [27] and electron impact ionization for the CF_2^+ channel [46,47] which observed a similar behavior. In a calculation for photoionization [9], this resonance was tentatively assigned to a t_2 shape resonance. Interestingly, increased cross sections in the vicinity of 35 eV were also measured for electron impact induced polar decay of CF_4 into $CF_3^+ + F^-$ and $CF_2^+ + F^- + F$ [68]. Thus, the phenomenon is not restricted to ionization but also present for excitation. Finally, respective peak structures were found for the CF_3^+ and CF_2^+ channels for positron impact ionization at the energy of about 28 eV [69]. This can be considered consistent with the present resonance energy if we take into account that for positron impact an energy gain of 6.8 eV occurs if positronium (Ps) is formed during the collision. This last observation makes the interpretation as a shape resonance questionable since electrons and positrons according to their opposite charge should experience different molecular potentials. Therefore, we have to conclude that there is no obvious explanation for the resonances which can explain the observations of all the existing studies and more experiments and theoretical calculations are necessary.

4 Conclusion

We have presented an (e, 2e + ion) triple coincidence study for ionization and fragmentation of CF_4 induced by low

energy electron impact at $E_0 = 67$ eV and 38 eV. Fragment channel resolved binding energy spectra and KER distributions were obtained for the fragments CF_3^+ and CF_2^+. In addition partial ionization cross sections as function of the impact energy were recorded.

For the CF_3^+ fragment essentially identical KER spectra are observed for the $\tilde{A}$, $\tilde{B}$, $\tilde{C}$ and $\tilde{D}$ ionic states. This confirms that fast decay of the higher ionic states into the $\tilde{A}$ state is preceding dissociation. The higher $\tilde{C}$ and $\tilde{D}$ states also dissociate into CF_2^+, and the KER distribution peaking at very low values for the $\tilde{C}$ state suggests a statistical decay. The $\tilde{D}$ state on the other hand shows rather high KER values around 1.5 eV suggesting a repulsive potential energy surface.

The CF_2^+ ion is observed at the lowest possible energy around the dissociation energy of 19.2 eV. Possible explanations are that the excitation of high vibrational levels of the $\tilde{B}$ state or excitation of autoionizing Rydberg states $CF_4^+(3t_2^{-1} nl)$.

The two applied projectile energies of 67 eV and 38 eV show slightly different state resolved ionization cross sections. For the energetically high $4a_1^{-1}$ state dissociating into CF_2^+ we observe reduced relative intensity for 38 eV compared to 67 eV. This is consistent with the regular behavior of the electron impact cross section being zero at threshold and rising roughly linearly. Therefore, the energetically highest states which are closer to threshold are affected strongest from the threshold effects.
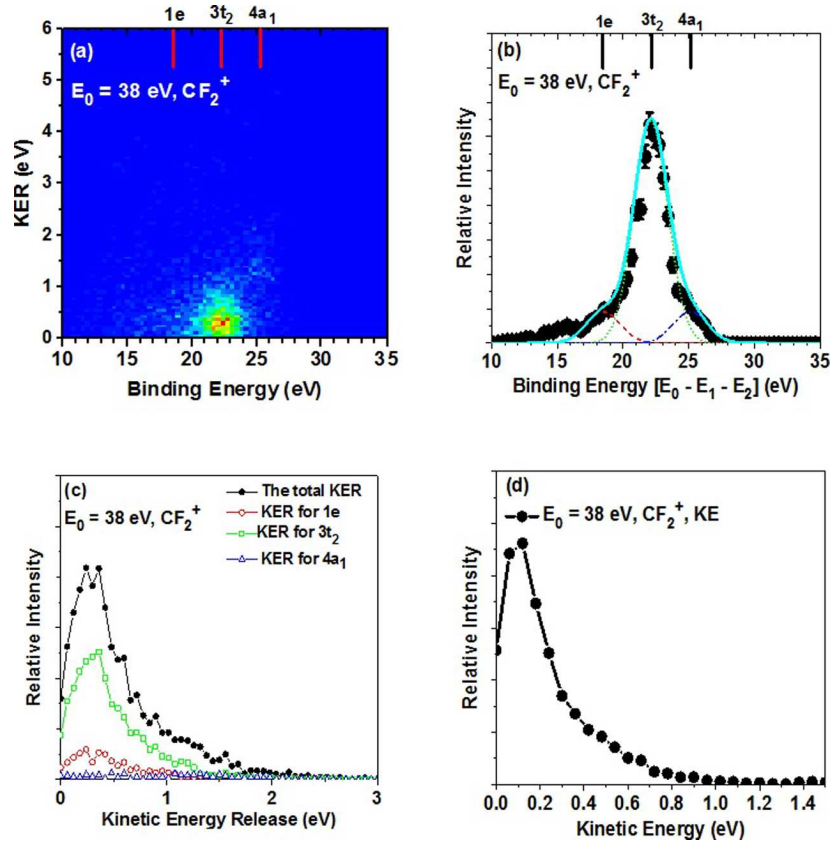
Fig. 5. As for Figure 4a–d but for electron impact energy of 38 eV.
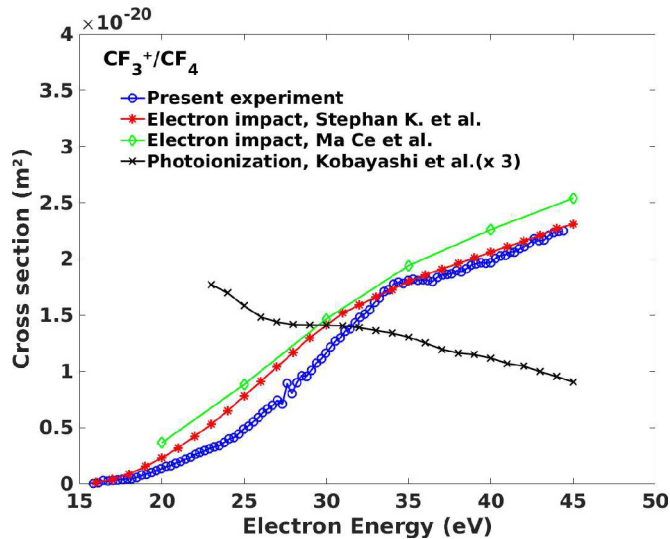

Fig. 6. Partial ionization cross section for formation of CF_3^+. Circular symbols (blue) show the current experimental data. Curves marked with crosses (black), stars (red) and diamonds (green) are data from references [27,46,47], respectively.
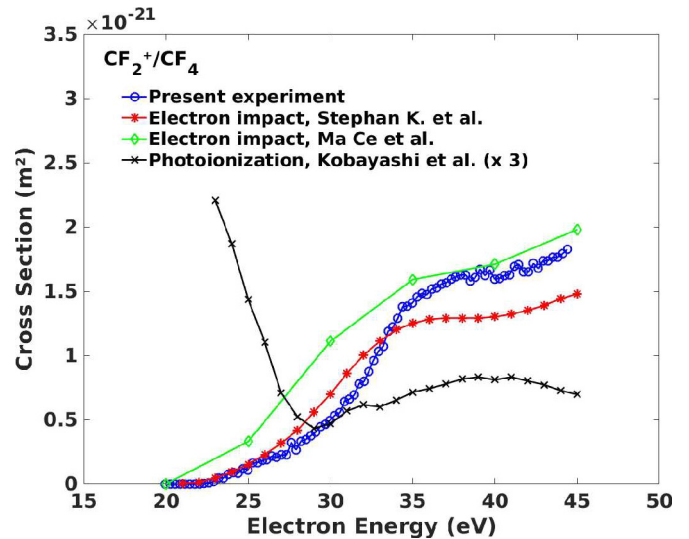
Fig. 7. Partial ionization cross section for formation of CF_3^+. Circular symbols (blue) show the current experimental data. Curves marked with crosses (black), stars (red) and diamonds (green) are data from references [27,46,47], respectively.

Finally, we have confirmed resonance structures observed in the partial ionization cross sections for both dissociation channels without being able to draw a clear conclusion about their origin. In order to get more insight in future, we plan to collect data with higher statistical significance and analyze angular distributions of the outgoing electrons. This will allow, e.g. to analyze beta parameters which show characteristic changes in the vicinity of resonances.

Altogether we have shown that the experimental technique of the reaction microscope enables (e, 2e + ion) triple coincidence studies which give detailed insight into electron impact induced ionization and dissociation of CF_4.

Author contribution statement

Khokon Hossen analyzed the results and drafted the manuscript. All authors participated in the experiment setting, discussion of the results, provided valuable comments, and contributed to the revision of the manuscript.

References

1. M.A. Huels, B. Boudaiffa, P. Cloutier, D. Hunting, L. Sanche, J. Am. Chem. Soc. **125**, 4467 (2003)
2. L.G. Christophorou, J.K. Olthoff, M.V.V.S. Rao, J. Phys. Chem. Ref. Data **25**, 1341 (1996)
3. R.P. Tuckett, Chem. Soc. Rev. **19**, 439 (1990)
4. J.C. Creasey, H.M. Jones, D.M. Smith, R.P. Tuckett, P.A. Hatherly, K. Codling, I. Powis, Chem. Phys. **174**, 441 (1993)
5. P.A. Hatherly, K. Codling, D.M. Smith, R.P. Tuckett, K.R. Yoxall, J.F.M. Aarts, Chem. Phys. **174**, 453 (1993)
6. L.C. Lee, X. Wang, M. Suto, J. Chem. Phys. **85**, 6294 (1986)
7. L.C. Lee, E. Phillips, D.L. Judge, J. Chem. Phys. **67**, 1237 (1977)
8. D.M.P. Holland, A.W. Potts, A.B. Trofimov, J. Breidbach, J. Schirmer, R. Feifel, T. Richter, K. Godehusen, M. Martins, A. Tutay, M. Yalcinkaya, M.A. Hada, S. Eriksson, L. Karlsson, Chem. Phys. **308**, 43 (2005)
9. E.M. Nascimento, L.E. Machado, L.M. Brescansin, M.-T. Lee, J. Electron Spectrosc. Relat. Phenom. **130**, 101 (2003)
10. J.A. Stephens, D. Dill, J.L. Dehmer, J. Chem. Phys. **84**, 3638 (1986)
11. I. Novak, A.W. Potts, F. Quinn, G.V. Marr, B. Dobson, I.H. Hillier, J.B. West, J. Phys. B: At. Mol. Opt. Phys. **18**, 1581 (1985)
12. T.A. Carlson, A. Fahlman, W.A. Svensson, M.O. Krause, T.A. Whitley, F.A. Grimm, M.N. Piancastelli, J.W. Taylor, J. Chem. Phys. **81**, 3828 (1984)
13. B.W. Yates, K.H. Tan, G.M. Bancroft, L.L. Coatsworth, J.S. Tse, J. Chem. Phys. **83**, 4906 (1985)
14. A.E. Jonas, G.K. Schweitzer, F.A. Grimm, T.A. Carlson, J. Electron Spectrosc. Relat. Phenom. **1**, 29 (1972)
15. A.J. Yencha, A. Hopkirk, A. Hiraya, G. Dujardin, A. Kvaran, L. Hellner, M.J.B. Ramage, R.J. Donovan, J.G. Goode, R.R.J. Maier, G.C. King, S. Spyrou, J. Electron Spectrosc. Relat. Phenom. **70**, 29 (1994)
16. D. Villaarejo, R.R. Herm, M.G. Inghram, J. Chem. Phys. **46**, 4495 (1967)
17. W.B. Peatman, T.B. Borne, E.W. Schlag, Chem. Phys. Lett. **3**, 492 (1969)
18. T. Baer, W.B. Peatman, E.W. Schlag, Chem. Phys. Lett. **4**, 243 (1969)
19. Y. Hikosaka, E. Shigemasa, J. Electron Spectrosc. Relat. Phenom. **152**, 29 (2006)
20. T. Masuoka, A. Kobayashi, J. Chem. Phys. **113**, 1559 (2000)
21. J.C. Creasey, I.R. Lambert, R.P. Tuckett, K. Codling, L.J. Frasinski, P.A. Hatherly, M. Stankiewicz, D.M.P. Holland, J. Chem. Phys. **93**, 3295 (1990)
22. B. Brehm, R. Frey, A. Küstler, J.H.D. Eland, Int. J. Mass Spectrom. Ion Phys. **13**, 251 (1974)
23. I.G. Simm, C.J. Danby, J.H.D. Eland, P.I. Mansell, J. Chem. Soc. Faraday Trans. 2 **72**, 426 (1976)
24. G.A. Garcia, H.S. Lose, L. Nahon, Rev. Sci. Instrum. **80**, 023102 (2009)
25. X. Tang, X. Zhou, M. Wu, Z. Gao, S. Liu, F. Liu, X. Shan, L. Sheng, J. Chem. Phys. **138**, 094306 (2013)
26. D.M. Smith, R.P. Tuckett, K.R. Yoxall, K. Codling, P.A. Hatherly, J.F.M. Aarts, M. Stankiewicz, J. Chem. Phys. **101**, 10559 (1994)
27. A. Kobayashi, A. Okaji, T. Masuoka, Chem. Phys. **298**, 107 (2004)
28. N. Saito, J.D. Bozek, I.H. Suzuki, Chem. Phys. **188**, 367 (1994)
29. N. Saito, J.D. Bozek, I.H. Suzuki, J. Phys. B: At. Mol. Opt. Phys. **28**, 3505 (1995)
30. R. Feifel, J.H.D. Eland, J. Chem. Phys. **125**, 194318 (2006)
31. M.K. Thomas, B.O. Fisher, P.A. Hatherly, K. Codling, M. Stankiewicz, M. Roper, J. Phys. B: At. Mol. Opt. Phys. **32**, 2611 (1999)
32. S.W.J. Scully, R.A. Mackie, R. Browning, K.F. Dunn, C.J. Latimer, AT0200294, http://www.iaea.org/inis/collection/NCLCollectionStore/_Public/33/060/33060763.pdf
33. W.R. Harshbarger, M.B. Robin, E.N. Lassettre, J. Electron Spectrosc. Relat. Phenom. **1**, 319 (1972)
34. N. Watanabe, D. Suzuki, M. Takahashi, J. Chem. Phys. **134**, 064307 (2011)
35. J.F. Ying, K.T. Leung, J. Chem. Phys. **100**, 7120 (1994)
36. K. Kuroki, D. Spence, M.A. Dillon, J. Chem. Phys. **96**, 6318 (1992)
37. W. Zhang, T. Ibuki, C.E. Brion, Chem. Phys. **160**, 435 (1992)
38. L. Boesten, H. Tanaka, A. Kobayashi, M.A. Dillon, M. Kimura, J. Phys. B: At. Mol. Opt. Phys. **25**, 1607 (1992)
39. W. Zhang, G. Cooper, T. Ibuki, C.E. Brion, Chem. Phys. **137**, 391 (1989)
40. J.W. Au, G.R. Burton, C.E. Brion, Chem. Phys. **221**, 151 (1997)

41. W.R. Harshbarger, E.N. Lassettre, J. Chem. Phys. **58**, 1505 (1973)
42. M.G. Curtis, I.C. Walker, J. Chem. Soc. Faraday Trans. 2 **85**, 659 (1989)
43. H. Nishimura, W.M. Huo, M.A. Ali, Y.-K. Kim, J. Chem. Phys. **110**, 3811 (1999)
44. I. Torres, R. Martínez, M.N.S. Rayo, F. Castaño, J. Chem. Phys. **115**, 4041 (2001)
45. H.F. Winters, M. Inokuti, Phys. Rev. A **25**, 1420 (1982)
46. K. Stephan, H. Deutsch, T.D. Märk, J. Chem. Phys. **83**, 5712 (1985)
47. C. Ma, M.R. Bruce, R.A. Bonham, Phys. Rev. A **44**, 2921 (1991)
48. I. Torres, R. Martinez, F. Castano, J. Phys. B: At. Mol. Opt. Phys. **35**, 2423 (2002)
49. S.S. Saini, U. Bhardwaj, Indi. Str. Res. J. **3**, 1 (2013)
50. T. Fiegele, G. Hanel, I. Torres, M. Lezius, T.D. Märk, J. Phys. B: At. Mol. Opt. Phys. **33**, 4263 (2000)
51. V.H. Dibeler, F.L. Mohler, Part J. Res. Natl. Bur. Std. **40**, 25 (1948)
52. M.R. Bruce, L. Mi, C.R. Sporleder, R.A. Bonham, J. Phys. B: At. Mol. Opt. Phys. **27**, 5773 (1994)
53. K.T. Leung, C.E. Brion, Chem. Phys. **91**, 43 (1984)
54. N. Watanabe, X. Chen, M. Takahashi, Phys. Rev. Lett. **108**, 173201 (2012)
55. K. Furuya, E. Koto, T. Ogawa, J. Phys. B: At. Mol. Opt. Phys. **34**, 1405 (2001)
56. X. Ren, T. Pflüger, M. Weyland, W.Y. Baek, H. Rabus, J. Ullrich, A. Dorn, J. Chem. Phys. **141**, 134314 (2014)
57. X. Ren, T. Pflüger, M. Weyland, W.Y. Baek, H. Rabus, J. Ullrich, A. Dorn, J. Chem. Phys. **142**, 174313 (2015)
58. S. Xu, X. Ma, X. Ren, A. Senftleben, T. Pflüger, A. Dorn, J. Ullrich, Phys. Rev. A **83**, 052702 (2011)
59. M.S. Banna, B.E. Mills, D.W. Davis, D.A. Shirley, J. Chem. Phys. **61**, 4780 (1974)
60. J. Ullrich, R. Moshammer, A. Dorn, R. Dörner, L.P.H. Schmidt, H.S. Böcking, Rep. Prog. Phys. **66**, 1463 (2003)
61. M. Weyland, X. Ren, T. Pflüger, W.Y. Baek, K. Bartschat, O. Zatsarinny, D.V. Fursa, I. Bray, H. Rabus, A. Dorn, Eur. Phys. J. Tech. Inst. **1**, 6 (2014)
62. C.R. Brundle, M.B. Robin, H. Basch, J. Chem. Phys. **53**, 2196 (1970)
63. K. Siegbahn, C. Nordling, G. Johansson, J. Hedman, P.F. Hedén, K. Hamrin, U. Gelius, T. Bergmark, L.O. Werme, R. Manne, Y. Baer, *ESCA applied to free molecules* (Amsterdam North-Holland Publ. Co., North-Holland, Amsterdam, 1969)
64. J.F.M. Aarts, S.M. Mason, R.P. Tuckett, Mol. Phys. **60**, 761 (1987)
65. M.R. Bruce, L. Mi, D. Soruco, R.A. Bonham, in *Proceedings of 18th International Conference on Phys. Elec. At. Coll. Amsterdam, North-Holland, Abstract* (1993), p. 315
66. M. Schmidt, R. Seefeldt, Int. J. Mass Spectrom. Ion Process. **93**, 141 (1989)
67. H. Deutsch, K. Leiter, T.D. Märk, Int. J. Mass Spectrom. Ion Process. **67**, 191 (1985)
68. L. Mi, C.R. Sporleder, R.A. Bonham, Chem. Phys. Lett. **251**, 252 (1995)
69. J. Moxom, D.M. Schrader, G. Laricchia, J. Xu, L.D. Hulett, Phys. Rev. A **62**, 052708 (2000)